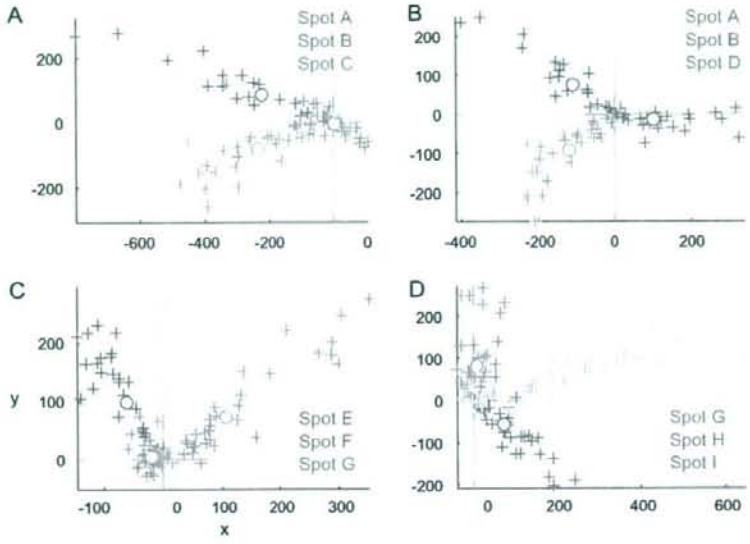

Figure 9. Distribution of MUs in the stimulus space indicating that MUs of each spots are clustered together. MUs and averaged MUs of activity spots are plotted on the stimulus space, that is, 100 dimensional space in which each dimension represents responses (spikes/s) to one of the 100 object images. We chose the 2D plane that includes points representing responses of averaged MUs of 3 spots to demonstrate clustering MUs of the 3 spots in each figure. Crosses, responses of MUs projected on the 2D plane. Open circles, responses of averaged MUs. Different colors indicate different spots. (*A*, *B*) Represent MUs of the spots in hemisphere H1. (*C*, *D*) Represent MUs of the spots in hemisphere H3.

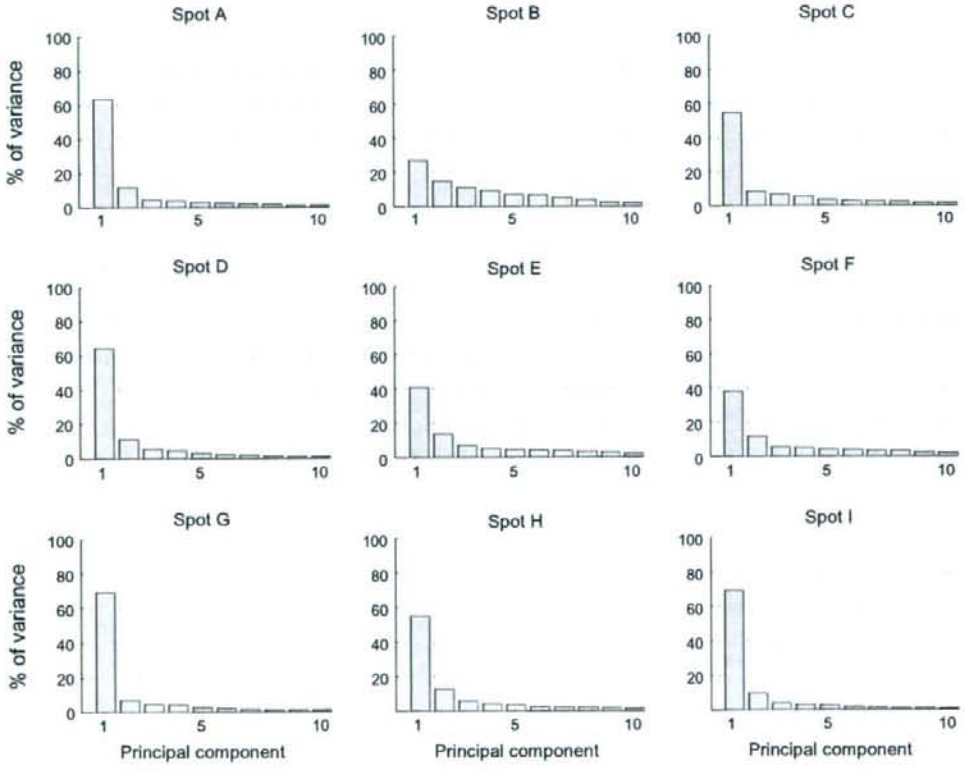

Figure 10. Contribution of each component in PCA of MUs of each spot in the stimulus space. Each figure represents the result of the analysis applied for one of the activity spots. Horizontal axes represent rank-ordered principal components. Only first 10 components are indicated. Vertical axes represent proportion of variance explained by each principal component.

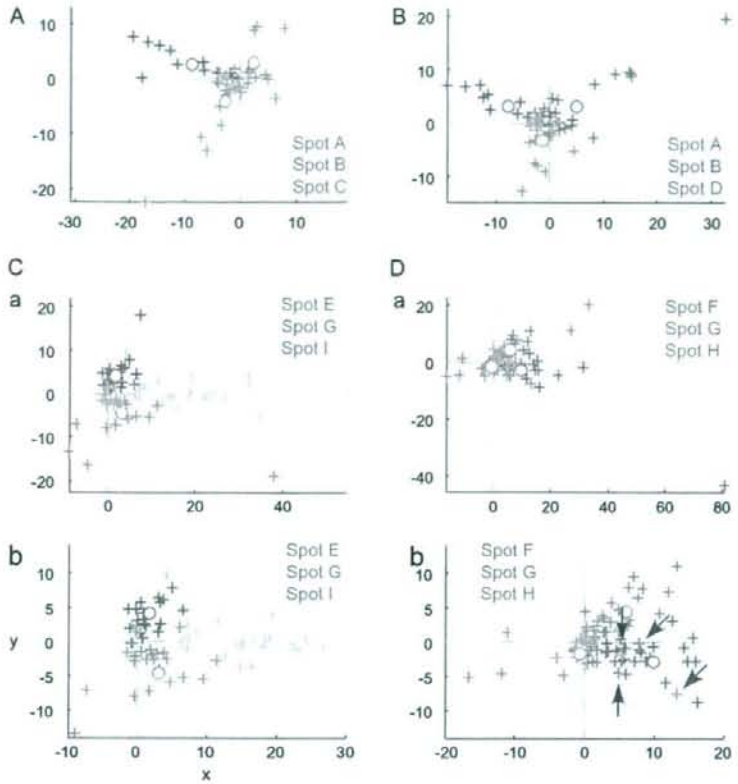

Figure 11. Distribution of single cells in the stimulus space. Responses of single cells (crosses) and average of single cells (open circles) are plotted on the stimulus space as in the case of MUs in Figure 9. We chose the 2D plane that includes points representing responses of average of single-cell responses of 3 spots. Different colors indicate different spots. (*A*, *B*) represent single cells of the spots in hemisphere H1. (*Ca*, *Da*) represent single cells of the spots in hemisphere H3. Some cells had very large responses compared with other cells, and it is difficult to capture overall patterns of distribution; spots in hemisphere H3 were plotted in magnified view (*Cb*, *Db*) as well.

(Table 1). These results indicate that each neuron, particularly the one in layers 1–4, shared the common property with an entire group of neurons within a spot.

The Spatial Arrangement of Clusters of Neurons with Common Response Properties

To address the question of whether or not common properties revealed by averaged MUs can be the result of columnar organization in area TE, we examined correlation for evoked responses between averaged MU and MU recorded from the same or different spots for averaged MU (see schematic drawings in Fig. 7*Aa*,*Ab*). First, the averaged MU highly correlated with MUs recorded from the same spots regardless of the depth of recording, although there was some tendency for the values of correlation coefficients to decrease with greater depth of recordings (Fig. 7*Aa*,*Ba*). The proportions of pairs of MUs and the averaged MU in a spot that had significant correlations calculated across the depth were 86.0% (98/114) and 86.2% (168/195) in hemispheres H1 and H3, respectively (for 100 object images, the proportions were 89.5% and 87.7% for H1 and H3, respectively [$P < 0.027$]) (Fig. 7*Aa*,*Ba*, lower panels). The values of the correlation coefficient were 0.44 ± 0.19 and 0.52 ± 0.27 (mean ± SD) for H1 and H3, respectively. In contrast, there were only a few pairs that showed significant correlation between MUs in one spot and averaged MU in the other spot, and there was no bias toward a particular depth of recording (Fig. 7*Ab*,*Bb*). The proportions of pairs of MUs and averaged MU with significant correlation across the depth were 18.1% (62/342) and 16.4% (128/780) (for 100 object images, the proportions were 21.9% and 11.8% for H1 and H3, respectively [$P < 0.027$]) (Fig. 7*Ab*,*Bb*, lower panels). The values of the correlation coefficient were 0.09 ± 0.13 and 0.05 ± 0.17 (mean ± SD) for H1 and H3, respectively. The minimum distances of the spot for an averaged MU and MUs in our experiments were 976 and 639 μm in H1 and H3, respectively, and the mean correlation values were already below the significance threshold ($P < 0.05$) at these distances (Fig. 7*Ac*,*Bc*). Thus, neurons at different depths had a common response property if they were in the same spot, but if the spots were even somewhat distant (e.g., 600 μm), the neurons did not share a common property. These results suggest that there is a columnar organization in area TE with respect to the common property in selectivity of neurons for 100 stimuli.

To find evidence for the columnar organization without calculating averaged MUs, we calculated the value of the correlation coefficient between the evoked responses of 2 single cells (Fig. 8*A*) and of 2 MUs (Fig. 8*B*) for those chosen

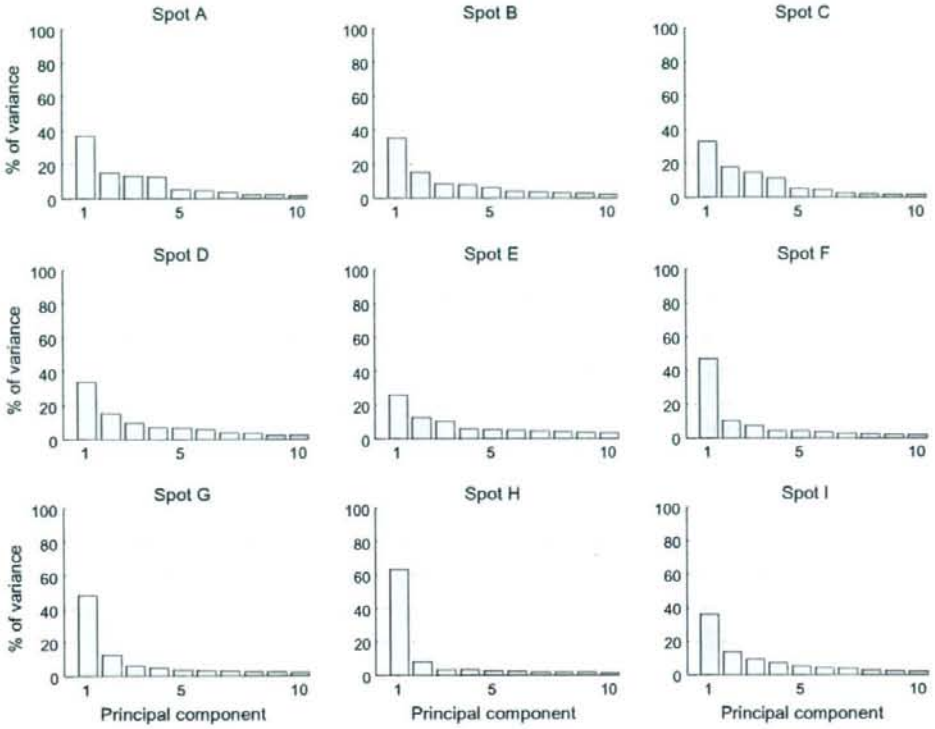

Figure 12. Contribution of each component in PCA of single cells of each spot in the stimulus space. Conventions are the same as in Figure 10.

from the same and different spots. On average, evoked responses of 2 single cells for 80 stimuli were not correlated irrespective of whether 2 cells were chosen from the same spots or from the different spots (Fig. 8*A*). Mean values of the correlation coefficient were 0.11 for the single-cell pairs from the same spots and 0.0084 for those from the different spots. Though these values were statistically significantly different (*t*-test, $P < 0.001$), the proportion of pairs that exceeded the threshold value of statistically significant correlation ($r = 0.22$, $P < 0.05$) was only 4.9% and 21.4% for pairs chosen from different and the same spots, respectively. Two MUs chosen from the different spots also showed low correlation in evoked responses. Contrary to the single-cell pairs, however, evoked responses of 2 MUs chosen from the same spots were highly correlated. Mean values of the correlation coefficient were 0.27 and 0.032 for the MU pairs from the same and different spots, respectively, and these values were statistically significantly different. Furthermore, the proportion of MU pairs that exceeded the threshold value of statistically significant correlation ($r = 0.22$, $P < 0.05$) was 55.7% for the pairs chosen from the same spots but was 8.8% for the pairs chosen from different spots. Because the common property across cells in the same spot are more emphasized in MUs than single cells, the correlation in object selectivity greatly increased from single-neuron pairs to MU pairs when these pairs were chosen from the same spots, whereas there was no difference in the values of the correlation coefficient for single-neuron pairs and MU pairs even if they were made from different spots.

Characterization of Common Properties across Cells in Activity Spots

Based on the comparison of object selectivity at the levels of single cells, MUs, and averaged MUs, we have suggested the existence of a common property among the cells in activity spots. However, we have not yet addressed the question of what the common property represented by individual spots was. Though it is difficult to identify a characteristic visual feature that explains the common property only from the results of object selectivity, we attempted some characterization of the common properties of activity spots. First, in the above analyses, we implicitly assumed that each spot is characterized by a response property. Alternatively, however, each spot may consist of a few subclusters of cells. Here, we consider that neurons in each cluster have their common property but that the properties of clusters are different from cluster to cluster. Even such a case, the results of the comparison of object selectivity at the level of single cells, MUs, and averaged MUs could be explained to some extent. We addressed this possibility by investigating how responses of MUs and single cells were distributed in the stimulus space. Here, the stimulus space represents a space made of 100 dimensions each representing evoked responses of MUs (or single cells) to one of 100 object images. If each activity spot is characterized by a response property, MUs and single cells from each spot form a single cluster in the stimulus space, and clusters are well separated from spot to spot. We first examined how MUs were distributed in the stimulus space. We plotted responses of averaged MUs of the activity spots in the

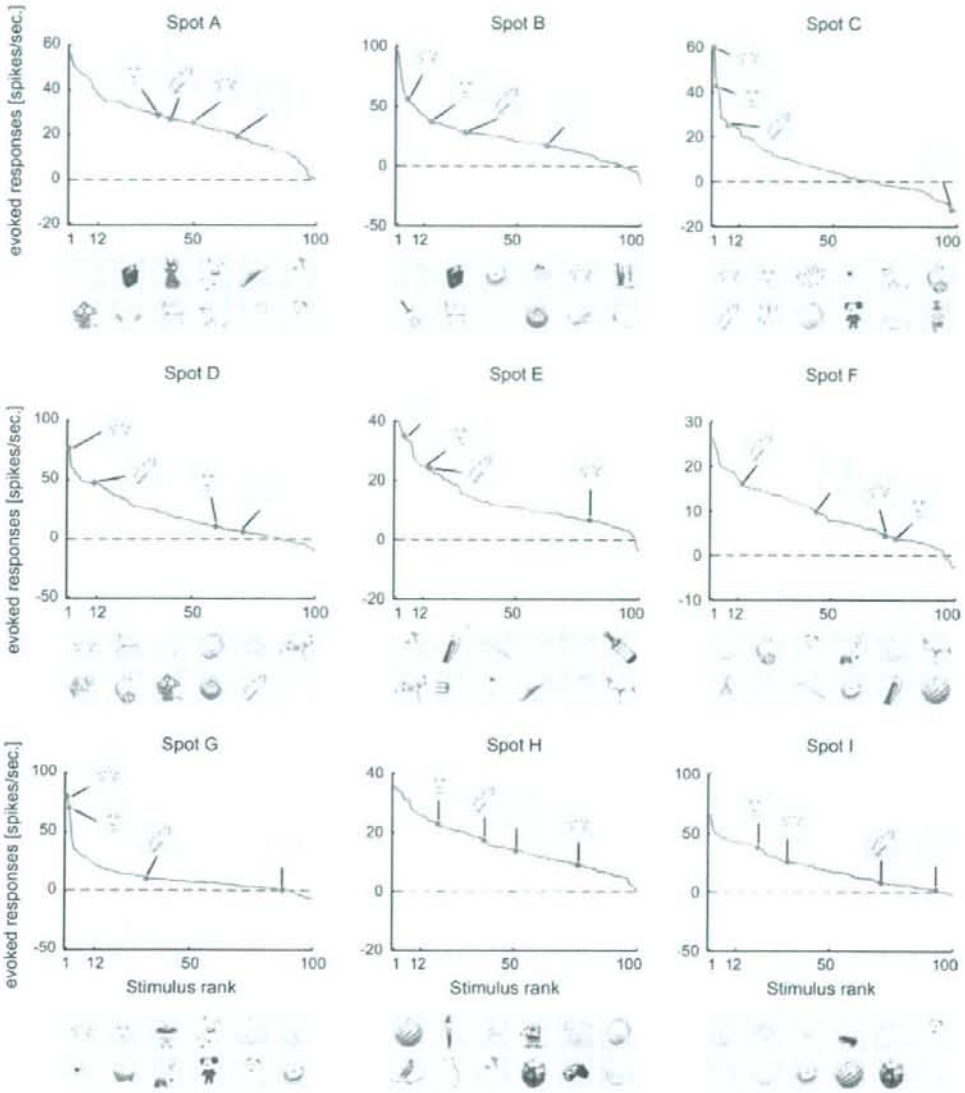

Figure 13. Rank-ordered stimulus responses of MUs (spikes/s) for each activity spot. Responses to faces and hands of human and monkey are indicated in each figure. The pictures below each figure represent top 12 object stimuli that are arranged in descending order from left to right. The upper row indicates the best to the 6th best images and the lower row indicates the 7th to the 12th images.

stimulus space and chose a 2-dimensional (2D) plane that includes the points representing averaged MUs of 3 spots (Fig. 9). In this way we visualized distribution of MUs of all activity spots in the stimulus space with 4 figures, each of which represented MUs of 3 of the activity spots (Fig. 9). We found that MUs of different spots formed well-separated clusters in the 2D plane. The MUs of each spot were distributed along the line connecting the average MU and the origin of the stimulus space (which corresponds to the point with no responses to any of objects). Thus, at least at the scale of the axes in which different spots are well separated, we found no indication of MUs with distinct response properties in individual spots. This result is further confirmed quantitatively with the principal component analysis (PCA). We applied PCA to MUs of each spot represented in the stimulus space (Fig. 10). Except for spot B, variance of the evoked responses of MUs in a spot was well explained by the first component, and contributions of the higher components were not very different from each other. Particularly, in 5 among 9 spots, the first component explains more than 60% of total variance. Second, we conducted the analyses of single-neuron responses in the same ways as in Figures 9 and 10 and investigated distribution of single cells in the stimulus space (Figs 11 and 12) because the analyses with MUs could not exclude a possibility that each MU consists of a set of subclusters of cells each being characterized by a different response property and MUs in a spot consist of the same set of subclusters.

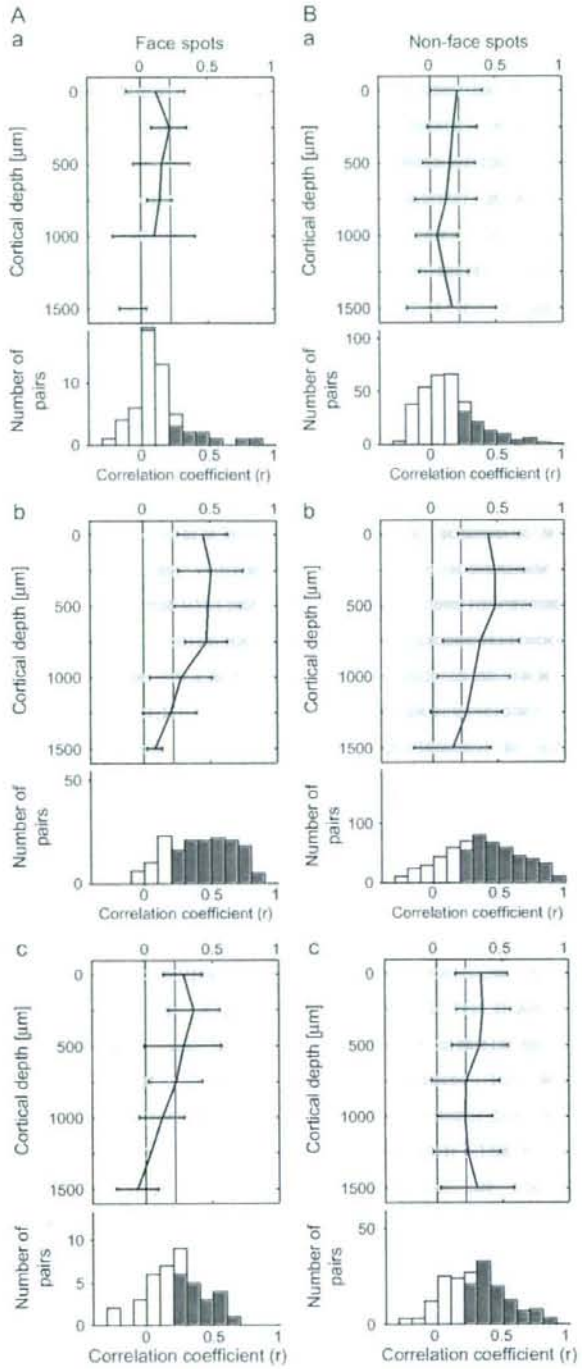

Figure 14. Comparison between face-selective spots and the other spots for similarity in stimulus selectivity. The results for spots C and G are represented in (*A*), and the results for the other spots are represented in (*B*). The other conventions are the same as in Figure 6. In (*Aa*, *Ba*), the values of the correlation coefficient were 0.12 ± 0.21 (mean ± SD, n = 55) and 0.13 ± 0.22 (mean ± SD, n = 323), respectively. The proportions of pairs that showed significant correlation were 18.2% and 27.2% for (*Aa*) and (*Ba*), respectively. In (*Ab*, *Bb*), the values of the correlation coefficient were 0.42 ± 0.24 (mean ± SD, n = 163) and 0.37 ± 0.29 (mean ± SD, n = 567), respectively. The proportions of pairs that showed significant correlation were 76.1% and 68.4% for (*Ab*) and (*Bb*), respectively. In (*Ac*, *Bc*), the values of the correlation coefficient were 0.22 ± 0.21 (mean ± SD, n = 40) and 0.29 ± 0.23 (mean ± SD, n = 178), respectively. The proportions of pairs that showed significant correlation were 47.5% and 59.0% for (*Ac*) and (*Bc*), respectively.

The results showed that single-cell responses of a spot were also well clustered and the clusters of single cells were well separated from spot to spot in 7 out of 9 spots (Figs 11 and 12). For example, in the case of spots A, B, C, and D, single-cell responses of one spot were clustered together, and the clusters of 3 spots were well separated (Fig. 11*A,B*). However, the results also showed that the remaining 2 spots (spots I and G) may consist of subclusters of cells with different response properties. For example, 4 spot G cells (arrows) were distributed differently from other spot G cells. They are even close to the cluster of single-cell responses of spot H in the 2D stimulus space (Fig. 11*Db*). Thus, though evidence was weak, we cannot exclude the possibility that some spots were characterized by a few numbers of common response properties.

In area TE, there are neurons specifically responding to faces and hands in addition to those responding to visual features that are less complex than object images (Gross et al. 1972; Desimone et al. 1984; Perrett et al. 1984; Tanaka et al. 1991; Kobatake and Tanaka 1994). Furthermore, a recent study combining fMRI and extracellular recordings revealed that face images activated localized region in IT cortex and that faces selectively activated neurons in the region (Tsao et al. 2006). This raised another question of whether or not only the cells specific for faces and hands cluster together and form activity spots. To address this question, we investigated object selectivity of averaged MUs of the activity spots with respect to the selectivity for faces and hands (Fig. 13). Spots C and G indeed seem to be specific for faces. In these spots, the first and second best stimuli are monkey and human faces, and responses to other objects were largely different from these face stimuli. Spot D may be face selective because the best stimulus was the monkey face, but the human face was the 60th best stimulus. The other 6 spots, however, were not specifically responsive to faces and hands. None of the best stimuli for these spots were faces, and many nonface objects were included in the top 12 stimuli. Face neurons are highly selective to faces but not selective among faces with different identities (Desimone et al. 1984). Thus, these results suggest that except spots C and G, activity spots represented visual features less complex than object images. In conclusion, existence of common properties among the cells in activity spots was not specific for the activity spots representing faces or hands. Furthermore, we found no quantitative differences between spots specific for faces (spots C and G) and the other nonface spots with respect to the results of the analysis of correlation among single cells, MUs, and averaged MUs (Fig. 14).

Specificity of the Response Property to Activity Spots Revealed by Intrinsic Signal Imaging

Because we recorded neuronal activities from the activity spots that were predetermined by intrinsic signal imaging, the above results may not reflect the general properties of area TE but the properties specific to the activity spots revealed by intrinsic

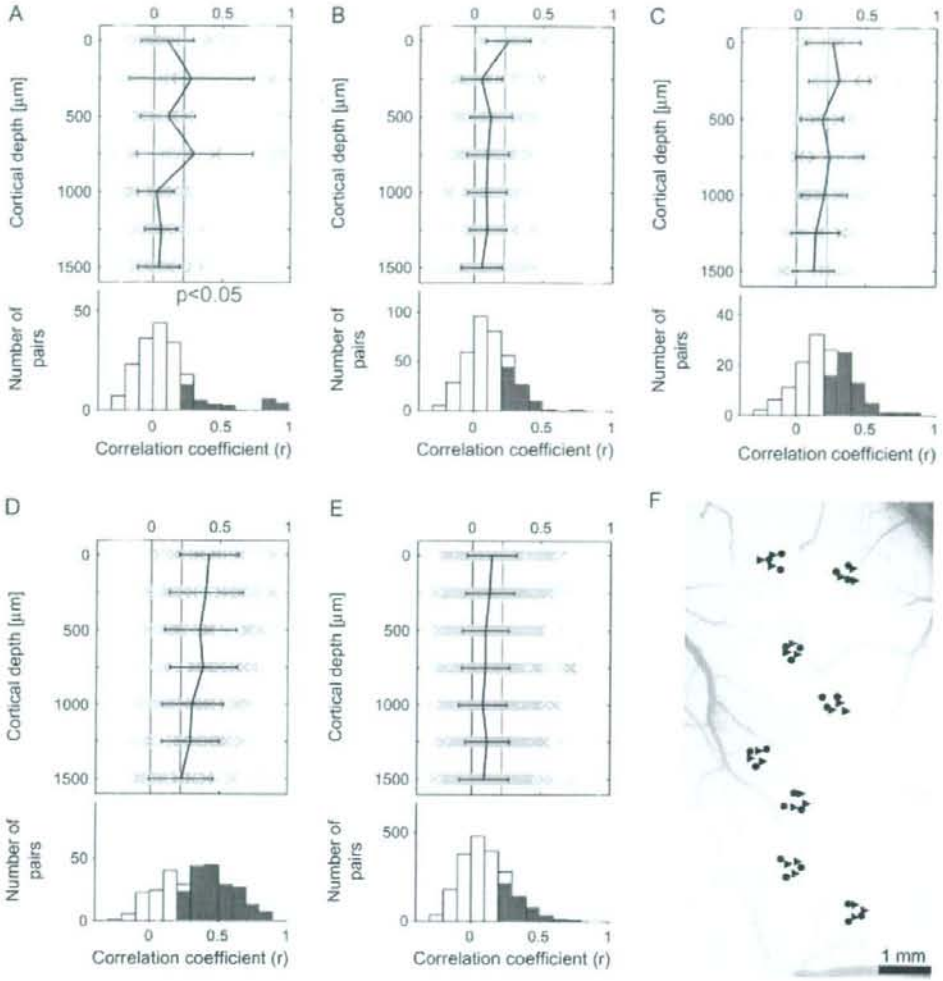

Figure 15. Similarity in stimulus selectivity between single isolated cells, MUs, and between single isolated cells and averaged MUs in hemisphere H2, where recording sites were randomly chosen without the guidance of intrinsic signal imaging. (*A*, *B*, *C*) correspond to Figures 6(*Aa*,*Ba*), (*Ab*,*Bb*), and (*Ac*,*Bc*), respectively. Conventions are the same as in Figure 6. (*D*, *E*) correspond to Figures 7(*Aa*,*Ba*) and (*Ab*,*Bb*), respectively. Conventions are the same as in Figure 7. (*F*) represents recording sites from hemisphere H2. Density of recordings within individual sites, and site-to-site distances, was adjusted nearly the same as in H1 and H3.

signal imaging. We addressed this issue by recording neuronal activities from another hemisphere (H2), in which we did not conduct intrinsic signal imaging beforehand but instead randomly chose 8 sites for extracellular recording (Fig. 15*F*). The results of the analysis of correlation among single cells, MUs, and averaged MUs for these sites were consistent with the results for the spots identified with intrinsic signal imaging and support the idea of the columnar organization in area TE: 1) the proportion of the pairs of a single neuron and the averaged MU with significant correlation (43.1%) was higher than the proportion of single-neuron pairs with significant correlation (18.1%) (Figs. 15*A*,*C*), 2) the correlation coefficient for the pairs of a single neuron and the averaged MU (0.20 ± 0.19, mean ± SD) were higher than that for the single-neuron pairs (0.10 ± 0.24), and 3) the proportion of pairs of an MU and the averaged MU with significant correlation, both within the same site, was as high as 65.7% (Fig. 15*D*), but the proportion was as low as 23.7% for pairs of an MU and the averaged MU at different sites (Fig. 15*E*). However, we found some tendency of the correlation being lower than that obtained from cells within the spots identified by intrinsic signal imaging. In particular, the proportion of MU pairs with significant correlation (22.7%) (Fig. 15*B*) was almost the same as the proportion of single-neuron pairs (18.1%) (Fig. 15*A*). This result was not due to the property specific to subpopulation of spots (Fig. 16). For the spots identified by intrinsic signal imaging (n = 9: 4 and 5 spots from H1 and H3, respectively), the distribution of spots shifted to the right (higher in values of the correlation coefficient) when MUs were used to calculate values of correlation coefficient (Fig. 16*A*). On the other hand, distribution did not show such shift for the randomly chosen sites (n = 8 from H2) (Fig. 16*B*). Based on this result, we

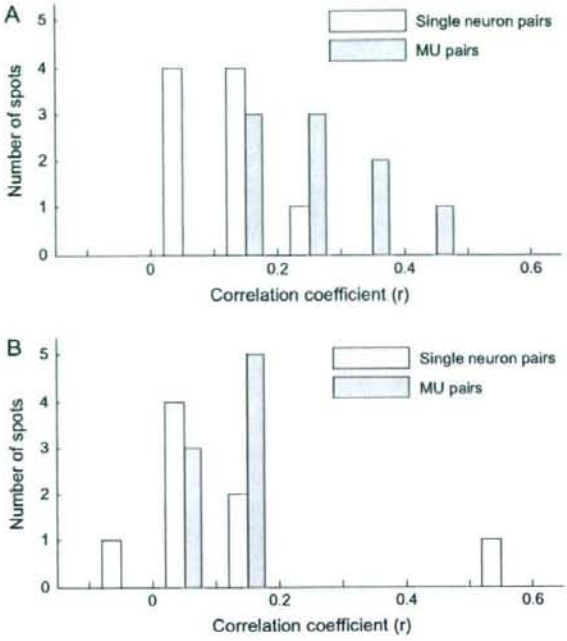

Figure 16. Relationship of object selectivity between single-neuron pairs and MU pairs for the spots identified by intrinsic signal imaging (*A*) and for the randomly chosen sites (*B*). The mean value of correlation coefficient (r) was calculated separately for each spot, and distribution of spots was plotted against the mean values of correlation coefficient. Total number of spots was 9 (4 spots from H1 and 5 spots from H3) for activity spots and 8 for randomly chosen sites.

suggest that IT cortex is organized in the region where neurons having similar response property are densely clustered and the region where those neurons are sparsely clustered (discussed later in detail).

Discussion

To examine the columnar organization in a cortical area, it is essential to use a set of stimuli that well characterizes functional properties of the cells in the area. However, such optimal stimulus sets are not available in many cortical areas, particularly in association cortices, and thus, firm evidence for columnar organizations is lacking in these areas. In the present study, we explored ways to examine columnar organizations in area TE without explicitly identifying the optimal stimulus set.

A general assumption is that because IT cortex is essential for object vision, evoked responses to a large number of object images should reflect functional properties of individual cells in IT cortex. On this basis, we examined selectivity of cells through their responses to 100 object images. We found that object selectivity is largely different from cell to cell, even if these cells are located in close vicinity (150 μm). However, this result does not eliminate the possibility of columnar organization in IT cortex. More importantly, we found that the selectivity of the averaged MU was similar to that of individual cells and MUs if they were recorded from the same spots (Figs 6*Ac*,*Bc* and 7*Aa*,*Ba*) but was different if cells and MUs were chosen from different spots (Fig. 7*Ab*,*Bb*). These results support the idea that a columnar organization does exist with respect to stimulus selectivity characterized by the averaged MUs.

The basis of the difference between cell-to-cell and cell-to-averaged MU similarity in object selectivity is well represented in tuning curves of individual cells where cells' evoked responses to object stimuli are plotted against the object stimuli arranged in the descending order of the preferred object images of the averaged MU (Fig. 17). Because there was cell-to-cell variability in object selectivity, different neurons had different peaks in the tuning curves. In most of the neurons, however, there was a general tendency that higher evoked responses were elicited by more effective object images for averaged MUs, and lower evoked responses were elicited by less effective object images for averaged MUs. These results could be explained by assuming that each neuron receives 2 different types of inputs: one specific for each neuron and the other common across the neurons within a spot (Fig. 18). The cell-specific inputs would be involved more in cell-specific responses to the object images that appeared as cell-specific peaks in the tuning curve, and the common inputs generate the general tendency of the tuning curve to be similar to that of averaged MUs. The cell-specific peaks in the individual tuning curves were different from cell to cell and were removed by averaging the MUs. Consequently, the common properties across the cells were disclosed in the averaged MUs (see also Appendix). The present study suggests that the common properties of a spot were different from those of the other spots if these spots were spaced at least 600 μm apart (Fig. 7*Ac*,*Bc*).Although common properties across the cells remained after averaging activities of MUs, it is possible that tuning specificity was greatly reduced by averaging and the averaged activities may lose stimulus selectivity that is meaningful for object image processing. To address this possibility, we calculated the sparseness index (SI) as a measure of tuning specificity for 80 object images (Rolls and Tovee, 1995). The SI is defined as

$$SI=\left(\sum_{i=1}^{n} r_i/n\right)^2 \Big/ \sum_{i=1}^{n} \left(r_i^2/n\right),$$

where r_i is the evoked response (spikes/s) to the ith stimulus in the set of n stimuli. It takes on a maximum value 1 if the all the stimuli activate the cell in identical evoked responses and takes $1/n$ if only one of n stimuli activates the cell. The SI of the evoked responses to the 80 object stimuli by single cells for H1 and H3 was, on average, 0.19 ± 0.18 (mean ± SD, n = 218). On the other hand, the SIs for MUs and averaged MUs for H1 and H3 were 0.33 ± 0.21 and 0.61 ± 0.18 (mean ± SD, n = 309 and 9 for MUs and averaged MUs, respectively). Thus, there was indeed a decrease in stimulus specificity. However, an SI of 0.6 is considered to be in the range indicating that the responses were still stimulus specific (Fig. 13; Rolls and Tovee 1995). The SIs calculated for the evoked responses of single cells, MUs, and averaged MUs in H2 were 0.17 ± 0.17 (n = 144), 0.17 ± 0.17 (n = 286), and 0.48 ± 0.20 (n = 8), respectively (mean ± SD).

The above discussion is based on the hemispheres where extracellular activities were recorded from activity spots that were predetermined by intrinsic signal imaging, and thus, the results may not reflect general properties of area TE. Here, we considered possible biases introduced by recording from specific sites in 2 aspects. First, because the stimuli used in intrinsic signal imaging were involved in 100 object images

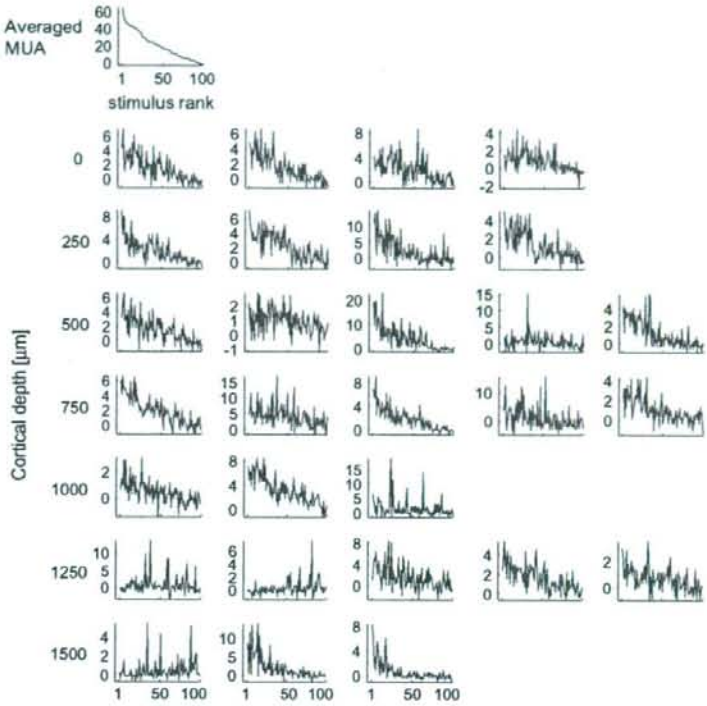

Figure 17. Tuning curves of the individual cells in a representative spot and the tuning curve of averaged MUs of the spot. The graph at the left upper corner represents the tuning curve of averaged MUs and the rests represent tuning curves of single cells at different depths. Depth of cells in each row is indicated at the left. Horizontal axes are rank ordered according to the magnitude of evoked responses of averaged MUs to the 100 object stimuli in descending order. Vertical axes represent mean firing rate (spikes/s).

examined for individual cells in the spots, correlation coefficients calculated for 100 object images may be biased to 20 object images used for intrinsic signal imaging. We calculated 2 values for correlation coefficients: one for 100 object images and the other for 80 object images where images used for intrinsic signal imaging were excluded. We did not find any qualitative difference in these 2 values as mentioned in the Results. Second, we considered a possibility that only part of IT cortex is organized in columns where neurons having similar response property are densely clustered, and intrinsic signal imaging extracted such columnar regions as activity spots. In hemisphere H2, where we did not conduct intrinsic signal imaging, the general tendencies of similarity among the cells were the same as those observed in the hemispheres with intrinsic signal imaging. In particular, the relationship between Figures 15(D) and (E) was consistent with the relationship between Figures 7(*Aa,Ba*) and (*Ab,Bb*), supporting the idea of columnar organization as a general functional structure in area TE. However, the values for correlation coefficients are lower than those values obtained from cells within the spots identified by intrinsic signal imaging. Specifically, similarity in object selectivity of MU pairs was almost the same as that of single-cell pairs for randomly chosen sites (Fig. 16*B*). There are 2 possible explanations for this difference caused by whether neuronal recordings were made from the activity spots or not. One explanation is that the recording sites were accidentally located at the border of 2 columns with different response properties. Previously with intrinsic signal imaging, we found that activity spots elicited by similar but different stimuli tend to partially overlap each other (Wang et al. 1996, 1998), and thus, the columnar organization in area TE would be like orientation columns in area V1 where response properties gradually change along the cortical surface (Tanaka 1996). Thus, it is not likely that the recording sites were located at the border of distinct columns. Another possibility is that a part of the cortex is organized in columns, but response properties of the neurons within the columns were not as similar as the activity spots identified by intrinsic signal imaging. In intrinsic signal imaging, the optical signal is proportional to the number of cells that responded to the presented stimulus, and activity spots were the sites that revealed local maxima of the optical signals (Tsunoda et al. 2001). Because of the small size of the optical signal, the activity spots could be biased to the regions that contained a large number of neurons that shared the same response properties. Thus, the cortex may be organized in a region where neurons with similar response properties were densely clustered (highly columnar region) and a region where neurons with similar response properties were sparsely clustered (less columnar region). The result showing the difference between optically identified spots and randomly chosen sites (Fig. 16) is consistent with this idea. Taking into account that IT cortex is highly plastic even in adults and that this plasticity is essential for the memory function of this area, the less columnar region could be considered as a reserved area for future use. The idea of mosaic organization of IT cortex with highly columnar and less columnar regions is interesting, but still speculative because

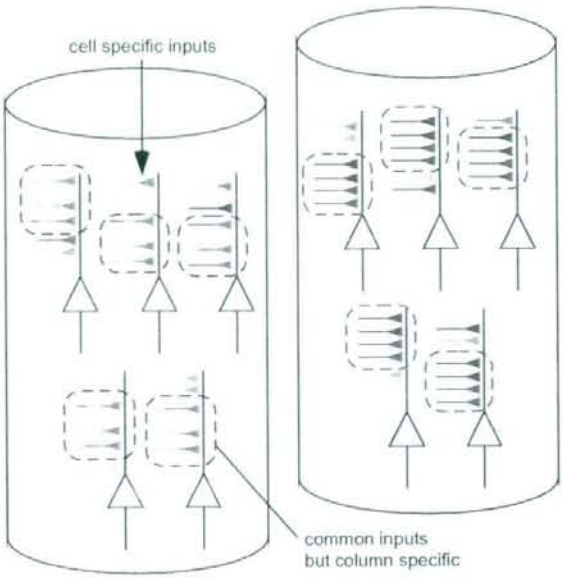

Figure 18. Schematic drawing of cell-specific inputs and inputs common among cells within a spot. Two columns are represented. The synaptic inputs demarcated by broken lines represent common inputs. These inputs are different from column to column. In this figure, the differences in common inputs for the 2 columns are indicated by the color of the inputs (left column, gray and right column, pink). Other inputs represent cell-specific synaptic inputs. We consider that these differences in synaptic inputs generate common and cell-specific response properties.

evidence provided by comparison between hemispheres with and without intrinsic signal imaging is indirect.

Although in an idealized model, a column with neurons of similar response properties extends from the cortical surface down to the white matter, this is not necessarily the case in real brains. In ocular dominance columns in area V1, for example, neurons exclusively responding to the visual stimulus given to one eye are found in layer 4 but not in superficial and deeper layers (Hubel and Wiesel 1972). Similarly in area TE, we found that neurons with stimulus selectivity significantly correlated with averaged MUs were more frequently found in layers above layer 4 (Fig. 6*Ac*,*Bc*). Thus, although there is a columnar spatial organization in area TE, there was some bias in superficial layers, including layer 4. In the case of area V1, critical response properties such as ocular dominance and orientation preference are primarily determined by the geniculate inputs to the area. Taking this into account, the bias to upper layers may reflect specificity of inputs to area TE from area TEO. In fact, it has been shown that area TEO projects not only to layer 4 but also to layers above layer 4 (Saleem et al. 1993).

The systematic analysis of columnar organizations in area TE was first conducted by Fujita et al. They obtained evidence suggesting columnar organization in area TE by using a stimulus simplification procedure to find the simplest visual feature for each cell (Fujita et al. 1992). It is likely that their stimulus simplification procedure led them to reach the common property across cells within a columnar region. Their stimulus simplification procedure (Tanaka et al. 1991), however, was not entirely objective, and thus, we cannot exclude the possibility that their analysis was biased. The importance of the present

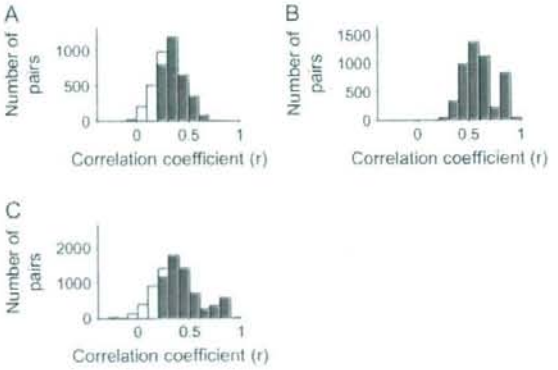

Figure 19. Demonstration showing increase of similarity in object selectivity by averaging activities of single cells. In each hemisphere, isolated cells were divided into 2 groups with equal number, and each group is averaged. A correlation coefficient was calculated between the evoked responses to 80 object images of these 2 averaged groups. Isolated cells were divided into 2 groups in 1000 different combinations, and resulting correlation coefficients were plotted in frequency distribution against the values of correlation coefficients. (*A*, *B*, *C*) were the frequency distribution obtained from hemispheres H1, H3, and H2, respectively. The mean and SD of the correlation coefficients were 0.35 ± 0.11, 0.59 ± 0.16, and 0.41 ± 0.20 for H1, H3, and H2, respectively. The column in red represents the pairs with significant correlation ($P < 0.05$, r 0.22).

study is that we showed the existence of one or potentially a few numbers of common properties across the cells in a columnar region with respect to object selectivity without such procedural bias.

Funding

Brain Science Institute, RIKEN. Funding to pay the Open Access publication charges for this article was provided by Brain Science Institute, RIKEN.

Notes

We thank Dr Kazushige Tsunoda for assistance with the surgical procedures and particularly for the procedure to expose the cortical surface. We also thank Ms Kei Hagiya for assistance during surgical procedures, Mr Hideyuki Watanabe for helping us for making the analysis software, and Ms Toshiko Ikari and Mr Mark Lescroart for comments on the manuscripts. *Conflict of Interest*: None declared.

Address correspondence to Manabu Tanifuji, Laboratory for Integrative Neural Systems, RIKEN Brain Science Institute, 2-1 Hirosawa, Wako-shi, Saitama 351-0198, Japan. Email: tanifuji@riken.jp

Appendix

In the present paper, we regarded the activities of an MU as the sum of activities of single cells. Although activities of single cells are indeed involved in an MUA, increase of object similarity in MUs and averaged MUs may be due to potential differences in single-cell activities and MUAs other than the number of cells that are involved. Here, we arbitrarily divided isolated single cells recorded within a spot into 2 groups, A and B, and examined whether the value of the correlation coefficient between evoked responses of averaged activities of group A and those of group B was higher than the values obtained for isolated neuron pairs. To avoid the 2 groups accidentally giving a high value of the correlation coefficient, we performed a permutation analysis where isolated cells were divided into groups A and B in various ways, correlation coefficients were calculated for individual grouping, and mean values ± SD of correlation coefficients were calculated (Fig. 19). The resulting values of correlation coefficients for H1, H3, and H2 were 0.32 ± 0.14, 0.60 ± 0.15, and 0.39 ± 0.21, respectively. These values were

higher than the mean value of correlation coefficients for isolated pairs of H1, H3, and H2, which were 0.11 ± 0.21, 0.15 ± 0.22, and 0.10 ± 0.24, respectively. These values were even larger than the mean value of MU pairs, which were 0.23 ± 0.20, 0.28 ± 0.26, and 0.10 ± 0.16 for H1, H2, and H3, respectively. These results support the idea that in MUs and in averaged MUs, cell-to-cell variability in object selectivity was removed and common properties were extracted.

References

Albright TD, Desimone R, Gross CG. 1984. Columnar organization of directionally selective cells in visual area MT of the macaque. J Neurophysiol. 51:16–31.

Arieli A, Grinvald A, Slovin H. 2002. Dural substitute for long-term imaging of cortical activity in behaving monkeys and its clinical implications. J Neurosci Methods. 114:119–133.

Baker C, Knouf N, Wald L, Fischl B, Kwang K, Benner T, Kanwisher N. 2004. Functional selectivity of human extrastriate visual cortex at high resolution. J Vis. 4:88–88.

Cheng K, Waggoner RA, Tanaka K. 2001. Human ocular dominance columns as revealed by high-field functional magnetic resonance imaging. Neuron. 32:359–374.

Desimone R, Albright TD, Gross CG, Bruce C. 1984. Stimulus-selective properties of inferior temporal neurons in the macaque. J Neurosci. 4:2051–2062.

Fujita I, Tanaka K, Ito M, Cheng K. 1992. Columns for visual features of objects in monkey inferotemporal cortex. Nature. 360:343–346.

Fukuda M, Moon CH, Wang P, Kim SG. 2006. Mapping iso-orientation columns by contrast agent-enhanced functional magnetic resonance imaging: reproducibility, specificity, and evaluation by optical imaging of intrinsic signal. J Neurosci. 26:11821–11832.

Gochin PM, Miller EK, Gross CG, Gerstein GL. 1991. Functional interactions among neurons in inferior temporal cortex of the awake macaque. Exp Brain Res. 84:505–516.

Gross CG, Rocha-Miranda CE, Bender DB. 1972. Visual properties of neurons in inferotemporal cortex of the macaque. J Neurophysiol. 35:96–111.

Hubel DH, Wiesel TN. 1962. Receptive fields, binocular interaction and functional architecture in the cat's visual cortex. J Physiol. 160:106–154.

Hubel DH, Wiesel TN. 1972. Laminar and columnar distribution of geniculo-cortical fibers in the macaque monkey. J Comp Neurol. 146:421–450.

Kobatake E, Tanaka K. 1994. Neuronal selectivities to complex object features in the ventral visual pathway of the macaque cerebral cortex. J Neurophysiol. 71:856–867.

Kreiman G, Hung CP, Kraskov A, Quiroga RQ, Poggio T, DiCarlo JJ. 2006. Object selectivity of local field potentials and spikes in the macaque inferior temporal cortex. Neuron. 49:433–445.

Malonek D, Tootell RB, Grinvald A. 1994. Optical imaging reveals the functional architecture of neurons processing shape and motion in owl monkey area MT. Proc R Soc Lond B Biol Sci. 258:109–119.

Mountcastle VB. 1957. Modality and topographic properties of single neurons of cat's somatic sensory cortex. J Neurophysiol. 20:408–434.

Perrett DI, Smith PA, Potter DD, Mistlin AJ, Head AS, Milner AD, Jeeves MA. 1984. Neurones responsive to faces in the temporal cortex: studies of functional organization, sensitivity to identity and relation to perception. Hum Neurobiol. 3:197–208.

Przybyszewski AW, Sato T, Fukuda M. 2008. Optical filtering removes non-homogenous illumination artifacts in optical imaging. J Neurosci Methods. 168:140–145.

Rolls ET, Tovee MJ. 1995. Sparseness of the neuronal representation of stimuli in the primate temporal visual cortex. J Neurophysiol. 73:713–726.

Saleem KS, Tanaka K, Rockland KS. 1993. Specific and columnar projection from area TEO to TE in the macaque inferotemporal cortex. Cereb Cortex. 3:454–464.

Tamura H, Kaneko H, Fujita I. 2005. Quantitative analysis of functional clustering of neurons in the macaque inferior temporal cortex. Neurosci Res. 52:311–322.

Tanaka K. 1996. Inferotemporal cortex and object vision. Annu Rev Neurosci. 19:109–139.

Tanaka K, Saito H, Fukada Y, Moriya M. 1991. Coding visual images of objects in the inferotemporal cortex of the macaque monkey. J Neurophysiol. 66:170–189.

Tsao DY, Freiwald WA, Tootell RB, Livingstone MS. 2006. A cortical region consisting entirely of face-selective cells. Science. 311:670–674.

Tsunoda K, Yamane Y, Nishizaki M, Tanifuji M. 2001. Complex objects are represented in macaque inferotemporal cortex by the combination of feature columns. Nat Neurosci. 4:832–838.

Wang G, Tanaka K, Tanifuji M. 1996. Optical imaging of functional organization in the monkey inferotemporal cortex. Science. 272:1665–1668.

Wang G, Tanifuji M, Tanaka K. 1998. Functional architecture in monkey inferotemporal cortex revealed by in vivo optical imaging. Neurosci Res. 32:33–46.

Yamane Y, Tsunoda K, Matsumoto M, Phillips AN, Tanifuji M. 2006. Representation of the spatial relationship among object parts by neurons in macaque inferotemporal cortex. J Neurophysiol. 96:3147–3156.

Available online at www.sciencedirect.com
ScienceDirect
Vision Research 48 (2008) 273–280
Vision Research
www.elsevier.com/locate/visres

Comparison of focal macular cone ERGs in complete-type congenital stationary night blindness and APB-treated monkeys ☆

Mineo Kondo *, Shinji Ueno, Chang-Hua Piao, Yozo Miyake, Hiroko Terasaki

Department of Ophthalmology, Nagoya University Graduate School of Medicine, 65 Tsuruma-cho, Showa-ku, Nagoya 466-8550, Japan

Received 1 August 2007; received in revised form 9 November 2007

Abstract

Focal macular cone electroretinograms (ERGs) and multifocal ERGs were recorded to study the macular function in patients with the complete-type of congenital stationary night blindness (cCSNB). The waveforms of the focal macular cone ERGs and the on- and off-responses of the multifocal ERGs in the cCSNB patients were similar to those recorded from monkey retinas treated with L-2 amino-4-phosphonobutyric acid (APB), suggesting that patients with cCSNB have a complete defect of the on-pathway even in the central retina. The results also demonstrated that there was a paradoxical positive response in the central retina of cCSNB patients, as compared to the negative full-field ERGs in the same subjects.

Keywords: Electroretinogram (ERG); Focal macular cone ERG; Congenital stationary night blindness (CSNB); Complete-type; APB (L-2 amino-4-phosphonobutyric acid)

1. Introduction

The complete-type of congenital stationary night blindness (cCSNB) is a non-progressive retinal disease characterized by congenital night blindness with a moderate decrease of the visual acuity and myopia (Miyake, Horiguchi, Suzuki, Kondo, & Tanikawa, 1997; Miyake, Yagasaki, Horiguchi, Kawase, & Kanda, 1986). The inheritance pattern of cCSNB is usually X-linked or autosomal recessive. It was recently reported that most X-linked cCSNB resulted from mutations in the *NYX* gene (Bech-Hansen et al., 2000; Pusch et al., 2000), and some cases of autosomal recessive cCSNB resulted from mutations in the *MGR6* gene (Dryja et al., 2005).

cCSNB patients have very characteristic electroretinograms (ERGs). When elicited by a bright stimulus after dark-adaptation, the ERGs are the negative-type with an a-wave of normal amplitude and a b-wave that is smaller than the a-wave. When a long-duration photopic stimulus is used, the b-waves of the ERGs of cCSNB patients are severely reduced while the off-response d-wave is well-preserved (Houchin, Purple, & Wirtschafter, 1991; Miyake, Yagasaki, Horiguchi, & Kawase, 1987; Young, 1991). These ERG waveforms are very similar to those in the monkey photopic ERGs after an intravitreal injection of 2-amino-4-phosphonobutyric acid (APB), which blocks neurotransmission from photoreceptors to the on-bipolar cells (Evers & Gouras, 1986; Knapp & Schiller, 1984; Sieving, Murayama, & Naarendorp, 1994). These results demonstrated that the defect in the neural pathway of cCSNB patients lies in the signal transmission from the photoreceptors to the depolarizing on-bipolar cells (DBCs) in both the rod and cone pathways. Recent ERG analysis using sinusoidal and ramping on/off flicker stimuli also indicated that the deficit in eyes with cCSNB is localized to the DBC pathway with no apparent involvement of the hyperpolarizing off-bipolar cells (HBCs) (Khan et al., 2005).

☆ *Grant support:* Grant-in Aid 14770952 (M.K.), and 14370557 (H.T.) from the Ministry of Education, Science, Sports and Culture, Japan.
* Corresponding author. Fax: +81 52 744 2278.
E-mail address: kondomi@med.nagoya-u.ac.jp (M. Kondo).

0042-6989/$ - see front matter © 2007 Elsevier Ltd. All rights reserved.
doi:10.1016/j.visres.2007.11.010

Although there are many electrophysiological studies on the full-field ERG in patients with cCSNB, there are very few studies on the macular function of eyes with cCSNB using either the multifocal or focal macular cone ERG techniques (Kondo et al., 2001; Leifert, Todorova, Prunte, & Palmowski-Wolfe, 2005). During our extensive studies of the complete and incomplete type of CSNB, we have been gaining the impression that the cone on-pathway may be functioning relatively well only in the central retina in cCSNB because these patients have relatively good visual function in the central field (Miyake et al., 1997; Terasaki et al., 1999).

The purpose of this study was to investigate the macular function of patients with cCSNB in more detail using focal macular cone ERGs and multifocal ERGs. To accomplish this, we separated the on- and off-responses of the photopic ERGs using long-duration photopic stimuli in the macular area of patients with cCSNB, and then compared the obtained waveforms with those recorded from monkey retinas in which the on-pathway was completely blocked pharmacologically by an intravitreal injection of L-2 amino-4-phosphonobutyric acid (APB).

2. Materials and methods

2.1. Patients with complete-type CSNB

From the patients with cCSNB examined in our clinic (Department of Ophthalmology, Nagoya University Hospital), we selected three patients who agreed to participate and were cooperative with the electrophysiological examinations (Table 1). All patients had poor night vision from birth and had no fundus abnormalities except for myopic changes. Their corrected visual acuities were 0.4, 0.4, and 0.6, and the rod branch of the dark-adaptation curve was missing as determined by psychophysical dark adaptometry. The full-field ERG rod responses were undetectable, and the rod and cone mixed maximal ERG had a negative-shape with no detectable oscillatory potentials.

An informed consent was obtained from the three patients after a full explanation of the procedures. All studies were conducted in accordance with the principles embodied in the Declaration of Helsinki.

2.2. Animals

Four rhesus (*Macaca mulata*) monkeys were studied under protocols approved by Nagoya University School of Medicine. All experiments were conducted in accordance with NIH guidelines on animal use and with the ARVO statement on the Use of Animals in Ophthalmic and Vision Research. The animals were anesthetized with intramuscular injection of ketamine hydrochloride (7 mg/kg, 5–10 mg/kg/h maintenance dose) and xylazine (0.6 mg/kg). The respiration and heart rate were monitored, and hydration was maintained by a slow, continuous infusion of lactated Ringer solution. The cornea was anesthetized by topical 1% tetracaine, and the pupil was dilated with topical 0.5% tropicamide, 0.5% phenylephrine HCL, and 1% atropine.

2.3. Drug application to animals

The drugs were injected into the vitreous with a 30-gauge needle inserted through the pars plana approximately 3 mm posterior to the limbus. The drugs (Sigma Chemical Co., St. Louis, MO) were dissolved in sterile saline and injected in amounts of 0.05–0.07 ml. The intravitreal concentration was 1–2 mM for L-2 amino-4-phosphonobutyric acid (APB) and 5 mM for *cis*-2, 3 piperidine dicarboxylic acid (PDA). Recordings were begun about 60–90 min after the drug injections, and studies were completed within 5 h. Although the drug effects are mostly reversible after a recovery period of several weeks, the results that are presented were recorded from the eyes not previously treated.

2.4. Focal macular cone ERG

Focal macular cone ERGs were elicited by stimulating the macula with small stimulus spots (Miyake, 1988b; Miyake, Shiroyama, Ota, & Horiguchi, 1988a). The position of the spot on the fundus was monitored during the recording with a modified infrared fundus camera. The Burian-Allen bipolar contact lens electrode (Hansen Ophthalmic Development Laboratories, Iowa City, IA) which was used to record the focal macular cone ERGs, allowed a clear view of the fundus on the television monitor. The luminances of the stimulus and the background were 30.0 cd/m^2 and 3.0 cd/m^2, respectively. A 5-Hz rectangular stimulus (100 ms-on and 100 ms-off) was used with a stimulus spot of 15 degrees in diameter. A total of 512 responses were averaged by a signal processor, and the time constant was 0.03 s with a 300-Hz high-cut filter. The ERG responses produced by this method are generated by the cone system, and the responses elicited by the spot stimuli are considered to be local responses (Miyake, 1988b; Miyake et al., 1988a).

2.5. Recording multifocal on- and off-responses

Our method for recording on- and off-responses of the multifocal ERGs has been described in detail (Kondo & Miyake, 2000; Kondo, Miyake, Horiguchi, Suzuki, & Tanikawa, 1998). In brief, multifocal ERGs were obtained with the VERIS system (EDI, San Mateo, CA). The stimulus array consisted of 61 hexagonal elements that were displayed on a CRT monitor (GDM, Sony, Tokyo, Japan) and driven at 75 frames/s. At a viewing distance of 27 cm, the subtense of the visual field was approximately 50°.

To obtain on- and off-responses with the VERIS system, we used consecutive white TV frames. Each hexagon was modulated between two stimulus patterns according to a binary m-sequence: eight consecutive white frames followed by eight consecutive dark frames (pattern A) or 16 consecutive dark frames (pattern B). In this stimulus setting, a stimulus is not continuously bright during its bright phase because the focal flash decays within a few milliseconds. However, there is evidence that a high-frequency train of flashes can roughly simulate the effects produced by a long-duration stimulus and thus can produce a corneal positive off-response (Saeki & Gouras, 1996; Young, 1991).

Based on our preliminary study, the following stimulus parameters were found to be suitable for eliciting maximal on- and off-responses from each local retinal area: stimulus intensity of 120 cd/m^2 with a duration of 8 frames (106 ms) on a 20 cd/m^2 background illumination. The m-sequence stimulation rate was, therefore, 4.7/s and the base interval was 213.3 ms (Kondo & Miyake, 2000; Kondo et al., 1998).

Table 1
Clinical characteristics of three patients with complete type CSNB

Case	Age	Sex	Inheritance pattern	Refractive error (*D*)	Visual acuity
Case 1	54	M	Autosomal recessive	−4.0	0.4
Case 2	20	M	X-linked	−9.5	0.4
Case 3	15	F	Autosomal recessive	−6.0	0.6

The signals were amplified by 100 K and filtered between 3 and 300 Hz (Grass, Quincy, MA). The data sampling rate was 1200 Hz. To reduce the artifacts due to eye movements, an "artifact rejection" algorithm (VERIS software, EDI) was used once (Marmor et al., 2003). The length of the m-sequence used was $2^{11}-1$. Thus, the total recording took 7.3 min, and it was divided into 16 segments.

For recording multifocal ERGs from monkeys, a modified ophthalmoloscopic technique was used to locate the projection of the fovea on the center of the stimulus pattern (Rangaswamy, Hood, & Frishman, 2003). This modified ophthalmoscope was kindly provided by Dr. L. Frishman (University of Houston). The position of the fovea was checked frequently before and after the multifocal ERG recordings.

2.6. Recording full-field ERGs

Full-field ERGs were recorded with long-duration stimuli (166 ms or 100 ms) using a densely-packed array of 102 green LEDs (525 nm peak wavelength; 50 nm at half-amplitude). The array was positioned at the top of the Ganzfeld dome and covered by a diffuser (Ueno et al., 2006). The LEDs were controlled by a digital function generator (WF1945, NF Corporation, Tokyo, Japan). The stimulus intensity and background illumination measured in the dome was 120 cd/m^2 and 40 cd/m^2, respectively. In the last experiment, the stimulus intensity and background illumination was set at 30 cd/m^2 and 3 cd/m^2, respectively, in order to compare the waveforms of full-field ERG and focal macular cone ERG at the same stimulus and background condition.

After 10 min of light adaptation, ERGs were recorded with a Burian-Allen bipolar contact lens electrode (Hansen Ophthalmic Development Labs, Iowa City, IA). A ground electrode was attached to the ipsilateral ear. Responses were amplified by 10 K and the bandpass was set to 0.3–1000 Hz. The data were digitized at 4.3 kHz. Twenty responses were averaged (Power Lab, AD Instruments, Castle Hill, Australia).

3. Results

3.1. Focal macular cone ERGs in cCSNB

Representative focal macular cone ERGs recorded from a myopic control (38-year-old man; refractive error, −5.50 D) and the three patients with cCSNB are shown in the left panel of Fig. 1. The waveforms from the three patients are clearly different from those of the myopic control: the amplitudes of the a-waves are normal, but the amplitudes of the following positive wave are smaller than the b-wave of the myopic control (see also Table 2). These changes resulted in a reduced b-wave to a-wave (b/a) ratio. In addition, the implicit times of the a- and b-waves in

Table 2
Amplitudes and implicit times of focal macular ERGs (FMERGs) from three patients with complete type CSNB and 15 patients with myopic controls

	Amplitude (μV)			Implicit times (ms)	
	a-wave	b-wave	b/a ratio	a-wave	b-wave
Case 1	2.4	2.4	1.0	21.4	47.2
Case 2	1.9	2.9	1.56	28.0	46.8
Case 3	2.4	3.1	1.29	28.0	59.5
Myopic controls ($n = 15$)	2.0 ± 0.5	5.1 ± 0.9	2.51 ± 0.44	19.6 ± 1.7	40.9 ± 3.0

Data in myopic controls are expressed as the mean ± SD.

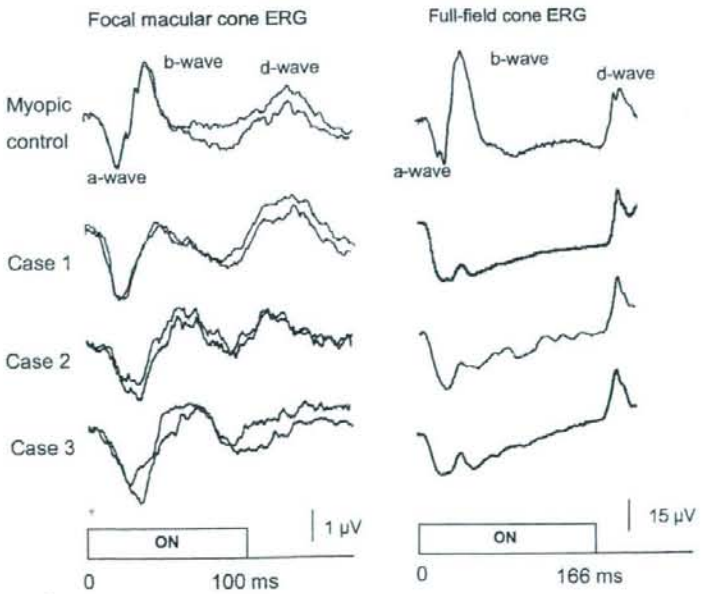

Fig. 1. Focal macular cone ERGs (left panel) and full-field ERGs (right panel) elicited by long duration stimuli recorded from a myopic control and three patients with complete-type congenital stational night blindness (cCSNB). Note that the amplitude ratios of the positive wave to the a-wave was <1.0 for the full-field ERG, but >1.0 for focal macular cone ERGs in the cCSNB patients.

cCSNB patients were prolonged (Table 2). The d-waves seen at the offset of the stimulus was not so prominent for both myopic controls and patients.

The full-field, photopic ERGs elicited by a long-duration stimulus (166 ms) from the same subjects are shown in the right panel of Fig. 1. In all three cCSNB patients, the b/a amplitude ratio was clearly <1.0 resulting in a "negative" ERG waveform.

3.2. Focal macular cone ERGs in monkey retina after APB

It is known that the on-response b-wave of the photopic long-flash ERG originates mainly from the neural activity of the cone depolarizing bipolar cells (DBCs) (Knapp & Schiller, 1984; Sieving et al., 1994). Based on the focal macular cone ERGs in the cCSNB patients, we thought that the function of cone on-pathway may be preserved to some degrees in the central retina of the cCSNB patients. To test this hypothesis, it was necessary to record the focal macular cone ERGs from the monkey retina after the cone on-pathway was completely blocked pharmacologically by APB, and to compare these waveforms with those from cCSNB patients.

The focal macular cone ERGs recorded from two rhesus monkeys before and after intravitreous injection of APB are shown in Fig. 2. After the APB injection, the a-wave amplitude became larger, and the peak time of the a- and the following positive wave became prolonged. The d-wave was slightly enhanced after APB. The ratio of the b-wave to the a-wave amplitudes became smaller than controls, but was still larger than 1.0 (monkey #1, 1.24; monkey #2, 1.33).

We initially interpreted this to indicate that remaining positive wave might be caused by an incomplete blockage of APB and thus injected more APB. However, the addition of APB did not change the waveforms of the focal macular cone ERGs, and the b/a amplitude ratio still remained greater than 1.0 even after increasing the APB concentration to twice the original concentration (2 mM).

The similarity in the waveforms between cCSNB patients and monkeys treated with APB indicated that the cone on-pathway seemed be completely blocked even in the central retina in cCSNB.

3.3. Multifocal on- and off-responses in cCSNB and APB-treated monkey

We also noted that the waveforms of photopic ERG with long duration stimuli were different between full-field cone ERGs and focal macular cone ERGs in cCSNB patients; the amplitude of remaining positive wave was still larger than that of the a-wave, whereas the amplitude ratio of the positive wave to the a-wave was always less than 1.0 for the full-field ERGs (Fig. 1). However, these differences in the waveform could be due to the different stimulus and recording conditions in the two methods. Therefore, we next compared these waveforms between the central and peripheral retinas directly in a patient with cCSNB. For

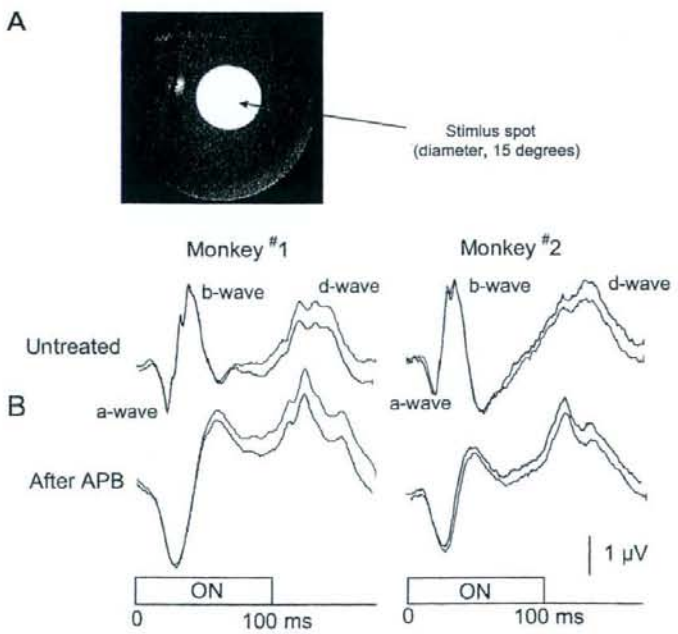

Fig. 2. Stimulus location and focal macular cone ERGs recorded from two monkeys. (A) Fundus photographs showing the stimulus spot. The 15° stimulus spot (diameter) was focused on the fovea. (B) Waveforms of focal macular cone ERGs before and after intravitreal injection of APB for two rhesus monkeys. Intravitreous concentration of APB was 1.0 mM.

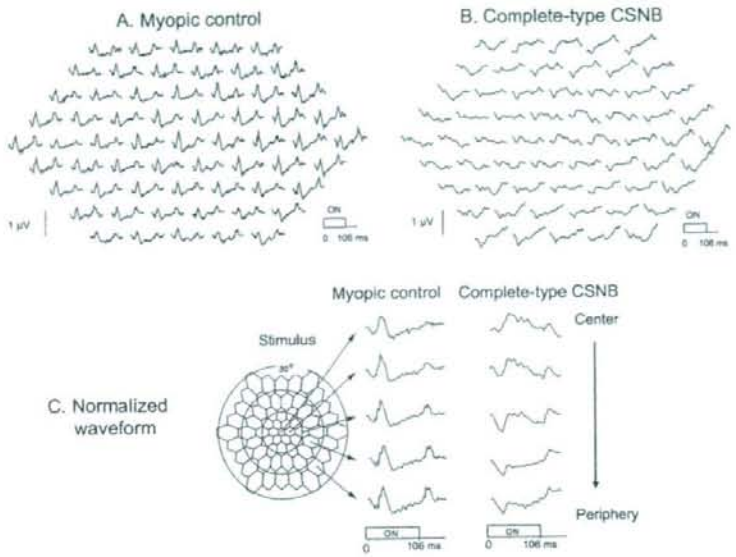

Fig. 3. Multifocal on- and off- responses using eight consequtive white frames. (A) Results from a myopic control. (B) Results from a patient with cCSNB (Case 1). (C) Normalized waveforms from five eccentric rings. Note that in cCSNB, the amplitude ratio of the positive wave to the a-wave is >1.0 in the central retina, but gradually become smaller towards to the periphery.

this purpose, we recorded the multifocal on- and off-responses (Kondo & Miyake, 2000; Kondo et al., 1998).

The multifocal on- and off-responses recorded from a representative myopic control (A), and a patient with cCSNB (B, Case 1 of Table 1) are shown in Fig. 3. It was clear that when compared to myopic control, the amplitudes of the positive wave are reduced at all locations in cCSNB. However, the amplitude of the positive wave is relatively preserved in the central retina, and the relative amplitude of the positive wave to the a-wave became small from the center to the periphery. The changes in the waveforms were clearly seen when the responses were grouped for each eccentric rings (Fig. 3C). The remaining positive wave is well preserved in the central retina, but gradually became smaller towards the peripheral retina. The amplitude ratio of the positive wave to the a-wave was >1.0 in the central retina, but <1.0 in the periphery. These findings are consistent with our combined findings of full-field ERG and focal macular cone ERGs in patients with cCSNB.

We also confirmed these results in a monkey retina after treatment with APB (Fig. 4). The remaining positive response was relatively large in the central retina, but the relative ratio of the positive wave to the a-wave gradually became smaller towards the periphery (Fig. 4C). These findings were quite similar to those in patients with cCSNB.

3.4. Origin of the remaining positive wave of photopic ERG at central retina

One question that still remained was the origin of the remaining positive component of the focal macular cone ERG seen even after blockage of cone on-pathway. To study the retinal origin of this component, we added PDA to block the neural activities of post-synaptic off-pathways and horizontal cells in monkeys. Fig. 5 shows the changes in the waveforms of photopic ERG with long duration stimulus before and after APB and PDA application for full-field and focal macular cone ERGs in a rhesus monkey. In this experiment, the same stimulus (30 cd/m^2) and background (3 cd/m^2) intensities were used for both full-field and focal macular cone ERGs, because the waveform of photopic ERG is dependent on the stimulus and background intensities (Kondo et al., 2000; Ueno, Kondo, Niwa, Terasaki, & Miyake, 2004). We found that after the PDA injection, the remaining positive wave of focal macular cone ERGs completely disappeared (lower traces of Fig. 5).

4. Discussion

We compared the waveform of focal macular cone ERGs recorded from cCSNB patients with those from APB-treated monkeys, and found that the waveforms were very similar: the amplitude of the a-wave was normal or slightly larger than control; a positive wave was still present after the a-wave, and the amplitude of this positive wave was larger than that of the a-wave; and the implicit time of the positive wave was delayed. These similarities in the waveform of focal macular ERG between the cCSNB patients and APB-treated monkeys suggested that the cone on-pathway is nearly completely blocked even in the central retina of the cCSNB patients.

Although the waveform of the a-wave and the following positive wave were very similar for cCSNB patients and

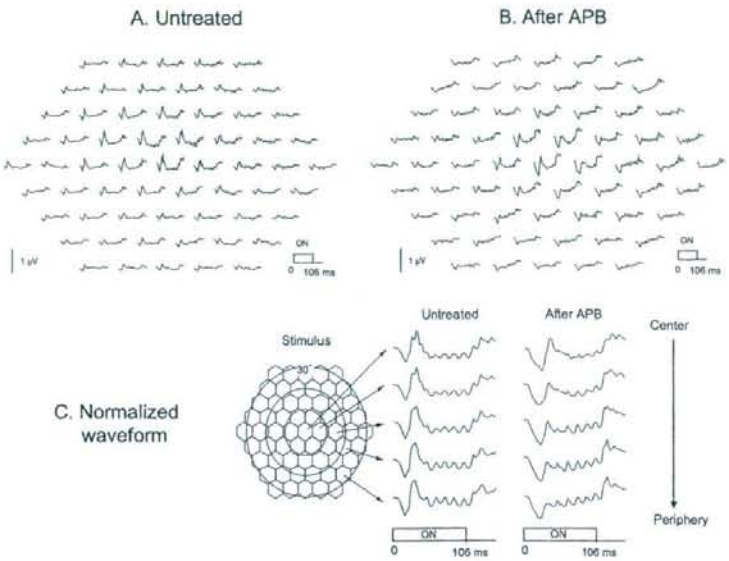

Fig. 4. Multifocal on- and off-responses before and after intravitreous injection of APB in a rhesus monkey. Intravitreous concentration of APB was 1.0 mM. Unstretched hexagonal elements (same size) are used for these monkey experiments. (A) Multifocal ERGs before APB. (B) Multifocal ERG after APB. (C) Normalized waveforms from five eccentric rings after APB application. The waveform after APB are very similar to those recorded from cCSNB patients.

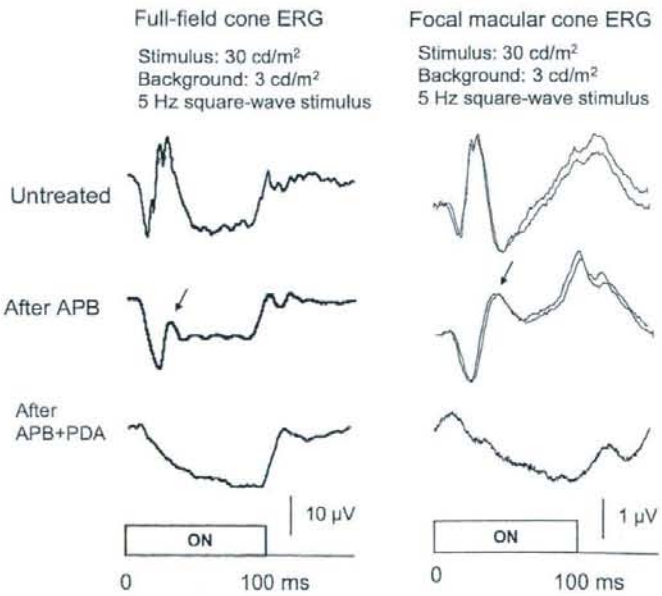

Fig. 5. Comparison in the waveforms of photopic ERG with long duration stimulus before and after APB and PDA application for full-field and focal macular cone ERGs in a rhesus monkey. Five hertz square-wave flickering stimulus of 30 cd/m^2 was presented on a background illumination of 3 cd/m^2 for both ERGs. After APB and PDA, the remaining positive wave at stimulus onset disappears completely for both ERGs (arrows).

APB-treated monkeys, the waveform of the d-wave at the offset of the stimulus was slightly different: the amplitude of the d-wave of the focal macular cone ERG was enhanced after the intravitreal injection of APB in monkeys, whereas the d-wave of focal macular cone ERG in cCSNB patients was not larger than that of myopic control. We do not know the reason for this difference in the waveform of the d-wave between the cCSNB patients and

APB-treated monkeys. However, it may be partly due to the differences between inherited human disease and the pharmacological animal model.

Although our electrophysiological study showed functional similarity between the retina of patients with cCSNB and APB-treated monkey retinas, there still remained the question of whether the retinal on-pathway is completely blocked in the retina of patients with cCSNB. Two psychophysical studies suggested that rod on-pathway may not be completely blocked in cCSNB patient (Allen et al., 2003; Young, Price, & Harrison, 1986).

We also found that even after a complete blockage of the cone on-pathway, there still remained a sizeable positive wave of the cone ERG in the central retina. The multifocal ERG results also demonstrated that the amplitude ratio of the positive wave to the a-wave was maximal in the central retina, and became gradually decreased towards the peripheral retina in a cCSNB patient and an APB-treated monkey supporting our combined findings of the full-field ERGs and focal macular cone ERGs. These results indicated that there is a unique spatial variation in the waveform of the cone ERGs. Other pharmacological studies in monkeys (Hare & Ton, 2002; Hood, Frishman, Saszik, & Viswanathan, 2002) also showed several spatial variations in the waveform of the cone ERGs using multifocal ERG technique, but they did not separate the on- and off-responses.

By adding PDA to APB, we found that the remaining positive wave of the cone ERG, which was seen even after blocking the cone on-pathway, originated from post-photoreceptor neurons which are sensitive to PDA, i.e., retinal neurons of the off-pathway or horizontal cells (Fig. 5). However, we could not identify exactly which retinal neurons/circuits contributed to this positive component. To identify the exact origin of this positive wave, further studies are needed using other pharmacological agents which affects specific retinal neurons.

Acknowledgments

The authors thank Laura J. Frishman of University of Huston for providing us her modified ophthalmoscope for multifocal ERG recordings for monkeys. We also thank Masao Yoshikawa, Eiichiro Nagasaka, Hidetaka Kudo of Mayo Corporation for technical helps.

References

Allen, L. E., Zito, I., Bradshaw, K., Patel, R. J., Bird, A. C., Fitzke, F., et al. (2003). Genotype-phenotype correlation in British families with X linked congenital stationary night blindness. *British Journal of Ophthalmology, 87*, 1413–1420.

Bech-Hansen, N. T., Naylor, M. J., Maybaum, T. A., Sparkes, R. L., Koop, B., Birch, D. G., et al. (2000). Mutations in NYX, encoding the leucine-rich proteoglycan nyctalopin, cause X-linked complete congenital stationary night blindness. *Nature Genetics, 26*, 319–323.

Dryja, T. P., McGee, T. L., Berson, E. L., Fishman, G. A., Sandberg, M. A., Alexander, K. R., et al. (2005). Night blindness and abnormal cone electroretinogram ON responses in patients with mutations in the GRM6 gene encoding mGluR6. *Proceedings of the National Academy of Sciences of the United States of America, 102*, 4884–4889.

Evers, H. U., & Gouras, P. (1986). Three cone mechanisms in the primate electroretinogram: Two with, one without OFF-center bipolar responses. *Vision Research, 26*, 245–254.

Hare, W. A., & Ton, H. (2002). Effects of APB, PDA, and TTX on ERG responses recorded using both multifocal and conventional methods in monkey. Effects of APB, PDA, and TTX on monkey ERG responses. *Documenta Ophthalmologica., 105*, 189–222.

Hood, D. C., Frishman, L. J., Saszik, S., & Viswanathan, S. (2002). Retinal origins of the primate multifocal ERG: Implications for the human response. *Investigative Ophthalmology & Visual Science, 43*, 1673–1685.

Houchin, K., Purple, R. L., & Wirtschafter, J. D. (1991). X-linked congenital stationary night blindness and depolarizing bipolar system dysfunction. [ARVO abstract]. *Investigative Ophthalmology & Visual Science, 32*, S1229 (Abstract No. 2741S).

Khan, N. W., Kondo, M., Hiriyanna, K. T., Jamison, J. A., Bush, R. A., & Sieving, P. A. (2005). Primate retinal signaling pathways: Suppressing ON-pathway activity in monkey with glutamate analogues mimics human CSNB1-NYX genetic night blindness. *Journal of Neurophysiology, 93*, 481–492.

Knapp, A. G., & Schiller, P. H. (1984). The contribution of on-bipolar cells to the electroretinogram of rabbits and monkeys. *Vision Research, 24*, 1841–1846.

Kondo, M., & Miyake, Y. (2000). Assessment of local cone on- and off-pathway function using multifocal ERG technique. *Documenta of Ophthalmologica, 100*, 139–154.

Kondo, M., Miyake, Y., Horiguchi, M., Suzuki, S., & Tanikawa, A. (1998). Recording multifocal electroretinogram on and off responses in humans. *Investigative Ophthalmology & Visual Science, 39*, 574–580.

Kondo, M., Miyake, Y., Kondo, N., Tanikawa, A., Suzuki, S., Horiguchi, M., et al. (2001). Multifocal ERG findings in complete type congenital stationary night blindness. *Investigative Ophthalmology & Visual Science, 42*, 1342–1348.

Kondo, M., Piao, C. H., Tanikawa, A., Horiguchi, M., Terasaki, H., & Miyake, Y. (2000). Amplitude decrease of photopic ERG b-wave at higher stimulus intensities in humans. *Japanese Journal of Ophthalmology, 44*, 20–28.

Leifert, D., Todorova, M. G., Prunte, C., & Palmowski-Wolfe, A. M. (2005). LED-generated multifocal ERG on- and off-responses in complete congenital stationary night blindness—A case report. *Documenta Ophthalmologica, 111*, 1–6.

Marmor, M. F., Hood, D. C., Keating, D., Kondo, M., Seeliger, M. W., & Miyake, Y. (2003). Guidelines for basic multifocal electroretinography (mfERG). *Documenta Ophthalmologica, 106*, 105–115.

Miyake, Y. (1988b). Studies of local macular ERG [in Japanese]. *Journal of Japanese Ophthalmological Society, 92*, 1418–1449.

Miyake, Y., Horiguchi, M., Suzuki, S., Kondo, M., & Tanikawa, A. (1997). Complete and incomplete type congenital stationary night blindness as a model of "OFF-retina" and "ON-retina". In M. M. LaVail, J. G. Hollyfield, & R. E. Anderson (Eds.), *Degenerative retinal diseases* (pp. 31–41). New York: Plenum Publishing.

Miyake, Y., Shiroyama, N., Ota, I., & Horiguchi, M. (1988a). Oscillatory potentials in electroretinograms of the human macular region. *Investigative Ophthalmology & Visual Science, 29*, 1631–1635.

Miyake, Y., Yagasaki, K., Horiguchi, M., & Kawase, Y. (1987). On- and off-responses in photopic electroretinogram in complete and incomplete types of congenital stationary night blindness. *Japanese Journal of Ophthalmology, 31*, 81–87.

Miyake, Y., Yagasaki, K., Horiguchi, M., Kawase, Y., & Kanda, T. (1986). Congenital stationary night blindness with negative electroretinogram: A new classification. *Archives of Ophthalmology, 104*, 1013–1020.

Pusch, C. M., Zeitz, C., Brandau, O., Pesch, K., Achatz, H., Feil, S., et al. (2000). The complete form of X-linked congenital stationary night blindness is caused by mutations in a gene encoding a leucine-rich repeat protein. *Nature Genetics, 26*, 324–327.

Rangaswamy, N. V., Hood, D. C., & Frishman, L. J. (2003). Regional variations in local contributions to the primate photopic flash ERG: Revealed using the slow-sequence mfERG. *Investigative Ophthalmology & Visual Science, 44*, 3233–3247.

Saeki, M., & Gouras, P. (1996). Cone ERGs to flash trains: The antagonism of a later flash. *Vision Research, 36*, 3229–3235.

Sieving, P. A., Murayama, K., & Naarendorp, F. (1994). Push-pull model of the primate photopic electroretinogram: a role for hyperpolarizing neurons in shaping the b-wave. *Visual Neuroscience, 11*, 519–532.

Terasaki, H., Miyake, Y., Nomura, R., Horiguchi, M., Suzuki, S., & Kondo, M. (1999). Blue-on-yellow perimetry in the complete type of congenital stationary night blindness. *Investigative Ophthalmology & Visual Science, 40*, 2761–2764.

Ueno, S., Kondo, M., Niwa, Y., Terasaki, H., & Miyake, Y. (2004). Luminance dependence of neural components that underlies the primate photopic electroretinogram. *Investigative Ophthalmology & Visual Science, 45*, 1033–1040.

Ueno, S., Kondo, M., Ueno, M., Miyata, K., Terasaki, H., & Miyake, Y. (2006). Contribution of retinal neurons to d-wave of primate photopic electroretinograms. *Vision Research, 46*, 658–664.

Young, R. S. L. (1991). Low-frequency component of the photopic ERG in patients with X-linked congenital stationary night blindness. *Clinical Vision Science, 6*, 309–315.

Young, R. S. L., Price, J., & Harrison, J. (1986). Psychophysical study of rod adaptation in patients with congenital stationary night blindness. *Clinical Vision Science, 1*, 137–143.

ISCEV ERG 30 – Rev 2008-09-01 (for posting: <iscev.org/standards>)

ISCEV Standard for clinical electroretinography (2008 update)

Marmor MF, Fulton A, Holder GE, Miyake Y (Chair), Brigell M, Bach M (for the International Society for Clinical Electrophysiology of Vision[1])

Affiliations

ABSTRACT:

This document, from the International Society for Clinical Electrophysiology of Vision (ISCEV), presents an updated and revised ISCEV Standard for clinical electroretinography (ERG). The parameters for stimulation and background adaptation have been tightened, and responses renamed in accordance with the flash luminance (in $cd \bullet s \bullet m^{-2}$). The ISCEV Standard specifies 5 responses: 1) Scotopic 0.01 ERG (rod response); 2) Scotopic 3.0 ERG (combined rod-cone response); 3) Scotopic 3.0 oscillatory potentials; 4) Photopic 3.0 ERG (cone response); 5) Photopic 3.0 flicker. An additional Scotopic 10.0 or 30.0 response is recommended.

Key Words: clinical standards, electroretinogram

Abbreviations: ERG – electroretinogram, ISCEV – International Society for Clinical Electrophysiology of Vision

Introduction

The full-field electroretinogram (ERG) is a widely used electrophysiologic test of

---

[1] This document was approved by ISCEV on 15 July, 2008 at the Annual General Meeting in Morgantown, WV, USA.

retinal function. In 1989, ISCEV standardized basic protocols so that comparable ERGs could be recorded throughout the world (1). Because of advances in ERG knowledge and techniques, this standard is reviewed regularly. This document supersedes the 2004 version (2). In this revision, we define background light and stimulus flash levels as single values, rather than ranges, to improve the consistency of ERG responses under the Standard. As in the 2004 Standard, we recommend an additional ERG to a stronger flash for the dark-adapted eye. We also propose a new format for specifying (naming) ISCEV Standard ERGs that will make reporting clearer.

The ERG Standardization Committee recognizes that older ERG recording equipment may not comply with some stimulus parameters, but hopes that this issue will resolve over time. Laboratories that do not fully comply with this current ISCEV Standard should indicate clearly in all reports and publications where their technique has differed.

An ISCEV Standard ERG includes the following responses, named according to conditions of adaptation and the stimulus (flash luminosity in $cd \bullet s \bullet m^{-2}$):

1) Scotopic 0.01 ERG (formerly "rod response")
2) Scotopic 3.0 ERG (formerly "maximal or standard combined rod-cone response")
3) Scotopic 3.0 oscillatory potentials
4) Photopic 3.0 ERG (formerly "cone response")
5) Photopic 3.0 flicker

Recommended additional response: either Scotopic 10.0 or Scotopic 30.0 ERG

The five basic ERGs represent the minimum ERG evaluation for clinical diagnosis. This standard describes simple technical procedures that allow reproducible recordings from patients of all ages except young infants. Different procedures can provide comparable ERGs. It is incumbent upon users of alternative techniques to demonstrate that their procedures do in fact produce signals that are equivalent in basic *waveform, amplitude, and physiologic significance* to the Standard.

It is intended that ISCEV Standard ERG protocols be used widely, but not to the exclusion of other tests or protocols that are not covered by this standard (see Table 1). We encourage electrophysiologists to extend test protocols to maximize the diagnostic value of the ERG for their patients and for clinical trials. ISCEV has also published guidelines for calibration of electrophysiologic equipment (3), guidelines for recording